sciendo

DOI 10.2478/ama-2024-0027

acta mechanica et automatica, vol.18 no.2 (2024)

HOMOTOPY PERTURBATION METHOD WITH TREFFTZ FUNCTIONS AND SIMCENTER STAR-CCM+ USED FOR THE ANALYSIS OF FLOW BOILING HEAT TRANSFER

Anna PAWIŃSKA*, Artur PIASECKI, Norbert DADAS***, Sylwia HOŻEJOWSKA****, Magdalena PIASECKA*****

*,****Faculty of Management and Computer Modelling, Kielce University of Technology, Al.Tysiąclecia Państwa Polskiego 7, 25-314 Kielce, Poland
**Faculty of Environmental Engineering, Geomatics and Renewable Energy, Kielce University of Technology, Al.Tysiąclecia Państwa Polskiego 7, 25-314 Kielce, Poland
,** Faculty of Mechatronics and Mechanical Engineering, Kielce University of Technology, Al. Tysiąclecia Państwa Polskiego 7, 25-314 Kielce, Poland

a.pawinska@tu.kielce.pl, apiasecki@tu.kielce.pl, ndadas@tu.kielce.pl, ztpsf@tu.kielce.pl, tmpmj@tu.kielce.pl

received 28 February 2023, revised 19 September 2023, accepted 20 September 2023

Abstract: This work presents experimental and numerical studies of heat transfer during cooling fluid flow in a group of five minichannels 1 mm deep. The main purpose was to determine the heat transfer coefficient on the contact surface between the fluid and the heated wall of the selected minichannel at subcooled boiling. The temperature distribution on the outer surface of the heated plate was measured by means of an infrared camera. Thermal and flow parameters were monitored by an appropriate data-acquisition system. The test section was placed horizontally with fluid flowing above the heated wall. The HFE-649, HFE-7100 and HFE-7200 working fluids were examined in the experiments. Simcenter STAR-CCM+ software was used for numerical analysis of heat transfer in the test section. Furthermore, a simplified two-dimensional (2D) model was proposed that designates subcooled boiling heat transfer during fluid flow in a central minichannel. The heat-transfer process in the heated plate and the working fluid was described using indicated partial differential equations with appropriate boundary conditions. The solution to the proposed system of equations led to the solving of two more inverse Cauchy-type problems. The classical Trefftz method (TM) and the homotopy perturbation method (HPM) combined with the TM allowed for obtaining temperature distributions in the heater and the fluid and consequently, the heat transfer coefficient at the heater–fluid interface from the Robin boundary condition. Comparison of the results from numerical simulation due to Simcenter STAR-CCM+ showed similar temperature distributions at the heated surface. The calculated heat transfer coefficients, by HPM and Simcenter STAR-CCM+, were validated using the 1D approach. Furthermore, the results from simulations in Simcenter STAR-CCM+ in the form of local temperatures of the heater were confronted with experimental data for comparison. Similar results were achieved.

Key words: heat transfer, minichannel, subcooled boiling, homotopy perturbation method, Trefftz method, Simcenter STAR-CCM+

1. INTRODUCTION

Various technical difficulties also arise as technology continues to develop and new technologies are constantly being introduced. One of the major challenges facing scientific and industrial institutions worldwide is cooling smaller and smaller electronic components while improving their capabilities and functionality. Designing small-sized, energy-efficient, effective and environmentally friendly refrigerant-based heat exchangers with a set of channels has become a priority in the industrial domain. Although high heat fluxes in miniaturised devices are commonly managed by intensifying heat transfer in the minichannels, the process is not fully understood. It requires innovative experimental studies, new mathematical models and computational methods that also include computational fluid dynamics (CFD) simulations.

It should be underlined that although important accomplishments have been made in the investigation of micro-scale flow boiling over the last two decades, most aspects related to heat transfer still remain unclear. Tibirica and Ribatski [1] provided a wide review of the literature on micro-scale and mini-scale flow boiling. The authors focussed on the transition from macro-scale to micro-scale, the heat transfer coefficient, critical heat flux, the pressure drop, flow patterns and the void fraction. The general characteristics of the experiments carried out by the researchers were provided. The presented results covered the data of investigations, with the test section having small-dimensional channels, which were tested for single channels and for a larger number of channels, including sets of channels. One of the conclusions was that the heat transfer coefficient achieved in the minichannel system is still not clear in the literature, and additional innovative studies are, therefore, necessary to investigate local phenomena. Such results would be useful for the development of mechanistic and predictive methods concerning micro and minichannel heat exchangers.

In Ref. [2], the flow boiling pressure drop and the flow patterns of R-600a in a multi-port horizontal extruded tube, with five rectangular channels and two rectangular/circular profiles, were studied. The average hydraulic diameter of the channels was 1.47

mm. The influence of mass flux and vapour quality on pressure drop was investigated, and the recorded two-phase flow patterns were analysed. The main results indicate the dependence of pressure drop on both mass and heat fluxes. The authors observed that the friction pressure gradient increased with increasing mass flux and vapour quality. The influence of heat flux on the frictional pressure drop was also noted.

Investigations on the boiling characteristics in the minichannel heat sink are described in Ref. [3]. The counter-flow interconnected minichannels were developed in the test section. Two minichannel heat sink configurations were used. The co-current minichannel structure size, with channel width of 1 mm, height of 4 mm, length of 30 mm and wall thickness of 1 mm was produced in the first version of the test section. The other construction differs from the first one, taking into account the width of the connected trench, which was 0.5 mm and the spacing equal to 4.5 mm. The results were related to heat transfer coefficients, pressure drop, two-phase flow patterns and temperature uniformity under various experimental conditions. The authors noted that with an increase in mass flux, the flow boiling performance is better than that of a low mass flux. Their explanation was that the connected groove could be effectively activated and mixing could be triggered. Among other findings, it was stated that increasing the supercooling can delay the boiling instability and increase the sensible heat of the fluid, which improves heat transfer performance. The authors also observed that the connected grooves in the test section cause the mixing of fluids between adjacent channels with reverse flow.

Flow boiling in three parallel minichannels with a common inlet and outlet area was studied in Ref. [4]. The internal dimensions of the minichannels were 0.25 mm wide, 0.50 mm deep and 32 mm long, whereas the wall between the channels was 0.25 mm wide. The minichannels were covered with a transparent cover, which allowed observation of flow structures. The authors focussed on examining the synchronisation between flow distributions in minichannels. This problem was analysed in the local area due to the analysis of the two-phase flow images and was also based on the process of synchronisation between inlet and outlet pressure fluctuations. The processes were investigated with the use of cross-recurrence plots. To recognise the similarity of flow patterns within the minichannels, the analysis of pixel brightness changes inside the minichannels was performed. The results revealed that the processes of synchronisation have a negative impact on water input and outlet temperature and inlet and outlet pressure oscillations. It was noticed that during synchronisation, a high amplitude of oscillations of temperature and pressure occurred. The authors stated that it was caused by reverse flow.

Numerical analyses of specific design solutions for minichannel devices have been the subject of an increasing number of research works. In Ref. [5] was showed the results of the CFD simulation using the COMSOL software. This software was used to simulate the convective heat exchange problem during forced water flow through the zone with the minichannel section. From the simulations, the local temperature of the fluid and that of the wall of the minichannel were calculated. Minichannels with a fixed length of 37.8 mm and a width of 1.615 mm had a height of 3.41 mm, 6.82 mm, 10.21 mm or 12.7 mm. As a result, local values of the Nusselt number were determined. The simulation was carried out for five different values of the Reynolds number. The fluid flow field and temperature distribution were also visualised. The frictional effects and the associated flow resistances were also analysed for various dimensions of the minichannel system.

In Ref. [6], the authors performed CFD modelling and a numerical analysis of fluid flow and heat transfer in a minichannel heat exchanger using Simcenter STAR-CCM+ software. The results of the numerical simulations were confronted with the data from the experiments. The main parameters that were measured during the experiments included the temperature distribution of the heater achieved by infrared thermography. The analyses covered the working fluid comprising two fluids (FC-72 and HFE-7100), the heater material (Haynes-230 alloy, aluminium and copper), the spatial orientation of the test section (vertical with fluid upflow and horizontal with fluid flow above the heater) and the number of minichannels (7, 9, 11 and 15). The calculations helped to indicate which parameters tested in terms of heat transfer turned out to be the most effective. Furthermore, a mesh dependency analysis was performed based on the grid convergence index to ensure the convergence stability of the numerical simulations.

Experimental data describing heat transfer during flow boiling in minichannels are needed to validate the results from numerical simulations. For more than two decades, the authors of this work performed calculations using various methods such as the simple 1D method [7], the 2D method described in this work and using the commercial software STAR-CCM+ [6] and ADINA [8].

This paper proposes two approaches to analyse the heat transfer in a test section with five rectangular minichannels and determine heat transfer coefficients at the heated plate–cooling fluid interface. The first approach used computational methods with Trefftz functions. A mathematical model was proposed in which the temperatures of the heated plate and all refrigerants were assumed to satisfy the Poisson and Fourier–Kirchhoff equations, respectively. The boundary conditions for both equations considered the results of experimental measurements. Determining the continuous temperature distributions of the heating plate and refrigerant leads to solving two inverse Cauchy-type problems in two contacting areas with different geometrical and physical parameters. Inverse problems belong to ill-posed problems [9], in which measurement uncertainties make the solution unstable. Inverse and ill-posed problems have been the subject of many works [10–13], and an overview of methods for solving Cauchy problems is given in Ref. [14]. For example, in Refs. [15–22], the Trefftz method (TM) or its modifications were used to solve direct and inverse problems that occur in engineering problems. In the TM (first described by Trefftz in 1926) [23], the unknown solution of a linear partial differential equation is approximated by a linear combination of functions (Trefftz functions or T-functions) that exactly satisfy the given differential equation. The coefficients of the linear combination are determined by minimising the error function that describes the mean square error between the approximate solution and the adopted boundary conditions. Trefftz functions combined with other methods, for example, Picard's method [22], radial functions [24] or homotopy perturbation method (HPM) [16, 20 and 21], are also used to solve non-linear differential equations.

This work uses two methods based on Trefftz functions for numerical calculations: the classical TM and a hybrid method that combines the HPM with Trefftz functions. Both methods use harmonic polynomials and are not limited by the number and type of boundary conditions. This greatly simplifies the calculations and makes these methods suitable methods for solving direct and inverse problems found in engineering. In the proposed approach, the solution to the differential equation (describing the heater temperature) was approximated by a finite sum of functions that

are linear combinations of the Trefftz functions. In the HPM, the unknown fluid temperature, the satisfying energy equation, is expressed as an infinite series of functions converging to the exact solution. The heat transfer coefficient at the heating plate–refrigerant interface was determined from the Robin boundary condition. The second approach used the CFD program, Simcenter STAR-CCM+. Numerical methods in CFD are designed to solve systems of nonlinear differential equations. The literature provides a good overview of mathematical models and numerical calculations for heat exchangers of various designs, as, for example, in the works [25–31]. The numerical simulation results were compared with those from methods based on Trefftz functions. Similar temperature distributions in the heated plate and heat transfer coefficients were obtained. The one-dimensional approach allowed for the validation of heat transfer coefficients obtained based on methods with Trefftz functions and from Simcenter STAR-CCM+ simulations.

2. EXPERIMENTS AND RESEARCH METHODOLOGY

2.1. Experimental rig

The experimental investigation was conducted in the own experimental set up. A view of the experimental rig is shown in Fig. 1 while its schematic diagram is shown in Fig. 2.

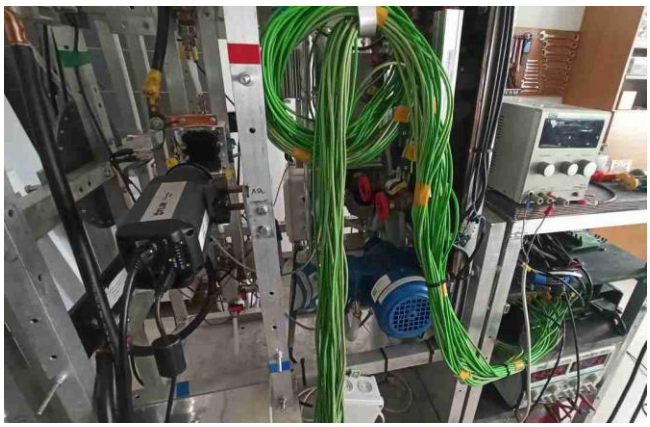

Fig. 1. A view of the experimental rig

In the main loop for the boiling process examination, the cooling fluid, i.e. HFE-649 (Novec-649 3M™ Novec™ [32]), HFE-7100 (3M™ Novec™ 7100 Engineered Fluid [33]) and HFE-7200 (3M™ Novec™ 7200 Engineered Fluid [34]), flows. Hydrofluoroethers (HFEs) are more environmentally friendly and, like fluorocarbon (FC), have zero (or close to zero) ozone-depletion potential (ODP). The significant difference, however, is a much lower global warming potential (GWP). According to the manufacturer [35], the FC-72 or FC-770 has more than 5,000 GWP, while the HFE fluids have the GWP even several times lower. For example, HFE-649, HFE-7000, HFE-7100 and HFE-7200 have a GWP of 1, 530, 320 and 55, respectively. Furthermore, FC fluids have a long atmospheric lifetime (ALR) and HFE-649, HFE-7000, HFE-7100 and HFE-7200 have ALRs of 0.014, 4.9, 4.1 and 0.77 years, respectively.

The main flow loop, besides the most important part, i.e. the test section, consists of the following elements: a circular pump (gear type, Tuthill), heat exchanger and pressure regulator. The most important set-up elements for the flow, pressure and temperature control and measurement are: mass flow meter (Coriolis type, Endress+Hauser), pressure meters (Endress+Hauser) and K-type thermoelements (Czaki Thermo-Product).

The data and image acquisition system includes an infrared camera A655SC FLIR (nominal accuracy ±2 °C or ±2% at measuring temperature range), a PC and two data acquisition stations (I/OTech DaqLab2005 and MCC SC-1608G) and a high-speed video camera (SP-5000M-CXP2, JAI). A lighting system consisting of LEDs (four LED panels of 50 W each) was applied to illuminate the flow of the working fluid along the minichannels. The power supply and control system consisted of a power supply, an ammeter and a voltmeter.

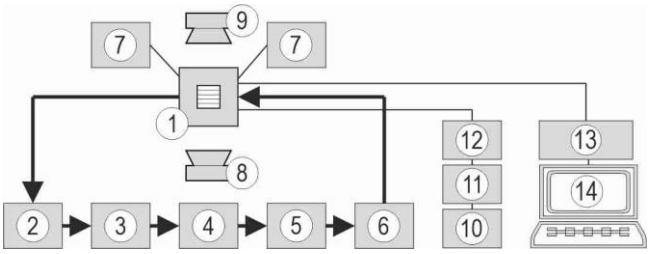

Fig. 2. A schematic diagram of the experimental rig – 1: test section, 2: heat exchanger, 3: compensation tank, 4: filter, 5: gear pump, 6: Coriolis mass flow meter, 7: pressure sensor, 8: infrared camera, 9: a high-speed video camera, 10: power supply system, 11: voltmeter, 12 -ammeter, 13: data acquisition station, 14: PC computer

2.2. Test section

The essential part of the experimental set up was the test section with a group of five parallel minichannels of rectangular cross-sections, each of pre-set depth 1 mm and width 6 mm, while their lengths taken into consideration are 43 mm. The schematic diagrams of the test section are shown in Fig. 3. The test section was placed horizontally with the fluid flowing above the heated wall. The heating element for the working fluid that flowed laminarly along the minichannels was a thin alloy plate stretched between two metal parts. This 0.1-mm-thick plate designated Haynes-230 is made of a high-temperature Ni–Cr–W–Mo alloy. The heater was powered by a heat source (the inverter welder acts as a regulated power supply) and was resistively heated, supplying heat to the fluid flowing in minichannels. The temperature distribution on the outer surface of the heated plate was measured by means of an infrared camera. Example thermograms on an outer side of the heated plate captured by an infrared camera are shown in Fig. 3a. It should be explained that a plate surface was coated with black paint of known emissivity (0.97). Example distributions of the temperature as a result of numerical computations based on experimental data are also shown in a half-image illustrated in Fig. 3a. Furthermore, a high-speed camera allowed recording flow structures through a transparent glass, which constitutes the opposite wall to the heated plate. Sensors of K-type thermoelements and pressure meters were mounted at the inlet and outlet of the minichannels.

Table 1 summarises the basic geometrical data of the test section. These data were used for calculations using methods with Trefftz functions and implemented into the Simcenter STAR-CCM+ program.

Tab. 1. Basic geometrical data of the test section

Basic geometrical data of the test section	Value (unit)
Number of minichannels in the test section	5
Length of the minichannels*	0.043 (m)
Thickness of the heated plate	0.0001 (m)
Depth of the minichannels	0.001 (m)
Width of a singular minichannel	0.006 (m)

*The length over which the temperature measurement is measured due to an infrared camera

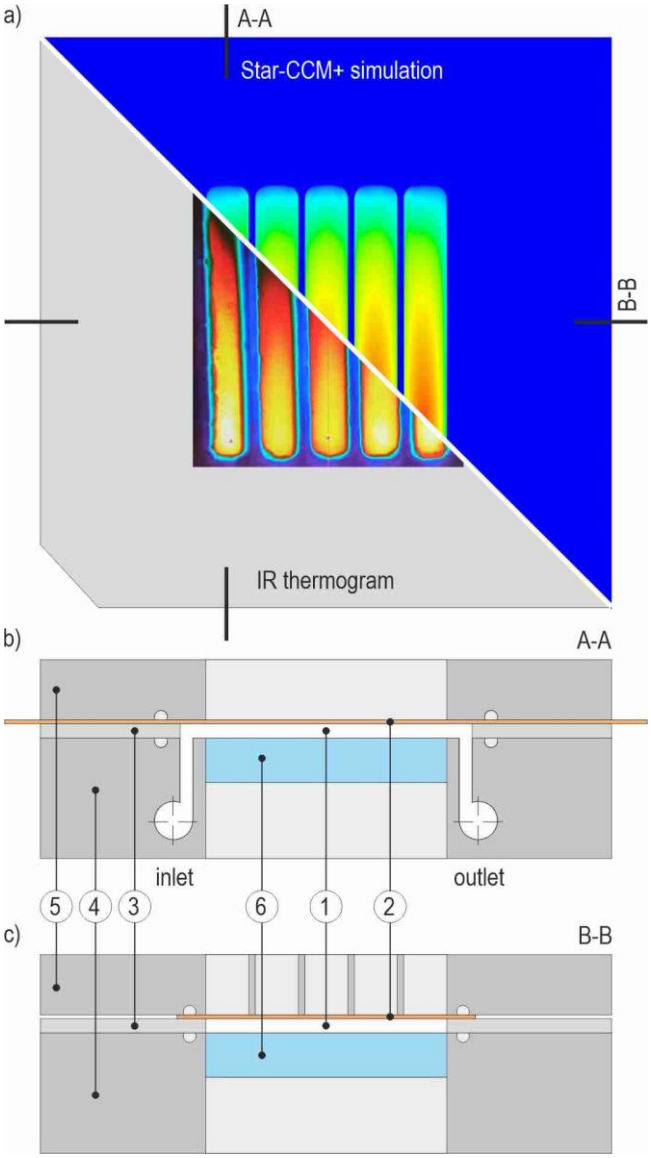

Fig. 3. Schematic diagram of the test section: (a) front view, (b) longitudinal section, (c) cross section; 1: minichannel, 2: heated plate, 3: Teflon spacer, 4: channel body, 5: front cover, 6: glass plate

2.3. Research methodology

A research pre-procedure is needed to ensure stabilisation of the set crucial experimental parameters. In this pre-procedure, the degassing of the fluid should be first ensured while it was circulating in a closed flow loop. Then, the initial temperature, pressure and flow parameters are set and stabilised during working fluid circulation. During the regular experimental series, there is a smooth increase in the current intensity supplied to the heated wall of the minichannels. The gradually increased heating power resulted in an increase in the temperature of the minichannel wall, and thus the cooling fluid in the minichannels is gradually heated along its flow. Sequentially, the values of pressure, temperature and mass flow of the working fluid and current supplied to the heated plate are collected in a 1-s interval, whereas single images of thermograms are captured by an infrared camera. Flow structures are simultaneously observed and recorded by a high-speed video camera.

According to the physical interpretation of the heat-transfer mechanism that occurs during the fluid flow, the experimental set up can be characterised as follows:

- After degassing and stabilising the experimental conditions, the subcooled liquid flows laminarly into an asymmetrically heated minichannel;
- In the beginning, when the heat flux increases, the heat transfer between the heating plate and the liquid proceeds via the single-phase forced convection;
- Further in the experiment, the increase in the heat flux results in boiling incipience in the minichannel, and subcooled boiling starts;
- When the heat flux continues to increase, nucleate boiling is in progress in the minichannel.

It should be underlined that the range of parameters characterising the selected series indicates that the data under analyses belong to the single-phase forced convection and the start of the subcooled
boiling region.

3. COMPUTATIONAL METHODS

3.1. Methods based on Trefftz functions

The 2D temperature distributions of the heated plate and cooling fluids were calculated with the classical TM and a hybrid method combining the HPM with the TM, respectively. This approach, which is a modification of that described in Ref. [36] considers two dimensions: one in the flow direction (x) and the other perpendicular to the flow (y) that relates to the thickness of the heated plate thickness δ_G and the minichannel depth δ_M.

The heat-transfer process in the heated plate, where $0 < x < H, 0 < y < \delta_G$, is assumed to be characterised by the Poisson equation, [36]

$$\lambda_G \left(\frac{\partial^2 T_G}{\partial x^2} + \frac{\partial^2 T_G}{\partial y^2} \right) = -q_V \quad (1)$$

where H: length of the minichannel, T_G: temperature of the heated plate, λ_G: thermal conductivity of the heated plate and q_V: heat flux supplied to the heated plate.

For Eq. (1), the temperature distribution at the plate's edge (T_{IR}) is known from infrared camera measurements. The remaining three edges (not in contact with the fluid) are insulated. The fluid flow in the minichannel is assumed to be laminar, with the velocity vector having one non-zero component $w(y)$ parallel to the flow direction. The fluid temperature for $0 < x < H, \delta_G < y < \delta_G + \delta_M$ satisfies the energy equation in the form:

$$\lambda_f \left(\frac{\partial^2 T_f}{\partial x^2} + \frac{\partial^2 T_f}{\partial y^2} \right) = \rho_f c_{p,f} w(y) \frac{\partial T_f}{\partial x} \quad (2)$$

where T_f: temperature of the fluid, λ_f: thermal conductivity of the liquid, ρ_f: density of the liquid and $c_{p,f}$: specific heat capacity of the liquid.

In Eq. (2), the temperatures of the fluid T_f and the heated plate at the fluid–plate contact surface are assumed to be equal, and that the fluid temperatures at the inlet $T_{f,in}$ and outlet $T_{f,out}$ of the minichannel are known. The boundary conditions adopted for Eqs (1) and (2) are shown in Table 2.

Tab. 2. Boundary conditions for the heated plate and the fluid

Section	Boundary conditions
Wall: $y = 0, 0 < x < H$	$T_G = T_{IR}$ $\frac{\partial T_G}{\partial y} = 0$
Wall: $x = 0, x = H, 0 < y < \delta_G$	$\frac{\partial T_G}{\partial x} = 0$
Contact wall: $y = \delta_G, 0 < x < H$	$T_f = T_G$
Inlet: $x = 0, \delta_G < y < \delta_G + \delta_M$	$T_f = T_{f,in}$
Outlet: $x = H, \delta_G < y < \delta_G + \delta_M$	$T_f = T_{f,out}$

Knowing the fluid and plate temperature allows for calculating the heat transfer coefficient from the formula:

$$\alpha(x) = \frac{-\lambda_G \frac{\partial T_G}{\partial y}(x, \delta_G)}{T_G(x, \delta_G) - T_{f,ave}(x)} \quad (3)$$

where: $T_{f,ave}$ is the average fluid temperature in the minichannel, calculated as in Ref. [36].

First, using the TM, the 2D temperature distribution of the heated plate was determined according to Ref. [36]. Then, the HPM with the TM was used to find the fluid temperature following the scheme below [20, 21].

In the HPM, differential Eq. (2) is written to distinguish two operators L (linear) and N (nonlinear), i.e.

$$LT_f = NT_f \quad (4)$$

For further calculations, it is assumed that

$$LT_f = \lambda_f \left(\frac{\partial^2 T_f}{\partial x^2} + \frac{\partial^2 T_f}{\partial y^2} \right) \quad (5)$$

$$NT_f = \rho_f c_{p,f} w(y) \frac{\partial T_f}{\partial x} \quad (6)$$

In the HPM, function $h(x, y, p)$ dependent inter alia on parameter $0 \leq p \leq 1$ satisfies the following equation:

$$(1 - p)[L(h) - L(u_0)] + p[L(h) - N(h)] = 0 \quad (7)$$

where u_0 denotes the initial approximation of the solution to Eq. (2).

Note that substituting p=1 in Eq. (7), Eq. (2) is obtained. Expanding the function $h(x, y, p)$ into a Taylor series about p, the solution to Eq. (2) can be written as follows:

$$T_f(x, y) = \lim_{p \to 1} h(x, y, p) = \sum_{i=0}^{\infty} h_i(x, y) \quad (8)$$

where $h_i(x, y) = \frac{1}{i!} \frac{\partial^i h(x, y, 1)}{\partial p^i}$.

Finally, the solution is approximated with a Taylor series truncated to M+1 components, i.e.

$$T_f(x, y) \approx \sum_{i=0}^{M} h_i(x, y) \quad (9)$$

By substituting Eq. (9) into Eq. (7) and equating the coefficients with successive powers of p, we obtain a system of equations containing the functions $h_i(x, y)$ as in Ref. [20]. We determine the functions $h_i(x, y)$ using the TM. The resulting fluid temperature approximately satisfies both Eq. (2) and the boundary conditions. The convergence of the solution obtained by the HPM, in the case of partial differential equations, has been proven, for example, in Ref. [37]. In practice, satisfactory results have already been obtained with three or four components of series (9), and the assumptions on the initial approximation u_0 can be weaker – it can be any function.

The experimental data used in calculations with the methods employing Trefftz functions and in Simcenter STAR-CCM+ are presented in Tabs. 3 and 4. In Tab. 3, the physical properties of the solids composed of the main elements of the test section are listed. Furthermore, in Tab. 4, the main physical properties of the working fluids and experimental parameters are shown.

Tab. 3. Physical properties of the solids composed of the main elements of the test section

Element of the test section				
Parameter/physical property	Haynes 230	Glass	Teflon	Aluminium
Density (kg·m^{-3})	8,970	2,500	2,160	2,702
Specific heat of the liquid (J·kg^{-1}·K^{-1})	400	840	702	903
Thermal conductivity (W·m^{-1}·K^{-1})	10.07	1.4	0.21	237

3.2. Numerical simulations in Simcenter STAR-CCM+

Numerical calculations were performed using Simcenter STAR-CCM+, version 2020.2.1 Build 15.05.010. This program let one perform calculations related to heat transfer, change of state of matter, fluid flow or mixing of different substances. After assuming the model of the test section and implementation, the data shown in Tabs. 3 and .4 into program, a desktop computer with an Intel Core i9 CPU (24 cores) and 256 GB of RAM clock speed at 3.50 GHz helped provide simulations.

4. RESULTS

4.1. Simulations due to Simcenter STAR-CCM+ and validation with experimental data

The temperature distribution in the test section as the results of numerical computations due to Simcenter STAR-CCM+ is shown in Fig. 4, respectively, for experiments with the fluids: HFE-649 (Fig. 4a,b), HFE-7100 (Fig. 4c) and HFE-7200 (Fig. 4d). In this figure, the computational grids assumed for numerical simulations are additionally enlarged to indicate more details in Fig. 4b.

Tab. 4. Main physical properties of the working fluids and experimental parameters

Physical properties of the working fluids			
Physical property	HFE-7200	HFE-7100	HFE-649
Density ($kg \cdot m^{-3}$)	1,430	1,532	1,510
Dynamic viscosity ($Pa \cdot s$)	0.00061	0.00061	0.00057
Specific heat of the liquid ($J \cdot kg^{-1} \cdot K^{-1}$)	1,214	1,118	1,183
Thermal conductivity ($W \cdot m^{-1} \cdot K^{-1}$)	0.068	0.069	0.069
Experimental parameters			
Fluid temperature at the inlet (°C)	16.2	16.60	13.8
Fluid temperature at the outlet (°C)	23.1	23.70	18.6
Temperature of an ambient air (°C)	24.5	21.5	18.7
Absolute pressure at the outlet (Pa)	94,503	106,045	109,471
Atmospheric pressure (Pa)	97,143	94,921	94,654
Mass flow rate of the fluid (kg/s)	0.00575	0.00580	0.00583
Heat flux supplied to the heater (W)	99.54	95.54	83.29

The velocity distribution in the fluid due to STAR-CCM+, shown in the longitudinal section of the central minichannels, based on the data from the experiment with HFE-649 are presented in Fig. 5. Additionally, computational grids are illustrated in enlarged sections of the inlet (left side) and the outlet (right side) of this figure.

For validation of the results from numerical simulations performed in Simcenter STAR-CCM+, the temperature of the heated plate on the outer surface that contacts ambient air was compared to the results known from the infrared thermography measurement. Figure 6 shows the dependence of the temperatures on the outer surface of the heated plate obtained from simulations and experimentation as a function of the distance from the minichannel inlet.

When the heater temperature vs the distance from the inlet was examined, a gradual increase in the temperature of the heated plate was observed with the increase in the distance in both relationships.

For a more detailed comparison, Tab. 5 shows the values of the mean relative differences (MRD) between the outer surface of the heated plate calculated by Simcenter STAR-CCM+ and measurements carried out by the infrared camera during the experiments.

Furthermore, the maximum absolute differences (MADs) were determined from the following formula:

$$\mathrm{MAD} = \max|\mathrm{f} - \mathrm{g}| \tag{10}$$

where f and g are functions.

The MAD values are also listed in Tab. 5.

When analysing the local temperatures of the outer surface of the heated plate obtained from numerical calculations in Simcenter STAR-CCM+ with the data obtained from the experiments shown in Fig. 6, it was stated that no significant disparities can be observed. The temperature distributions are very similar in both cases. Furthermore, the MRD between the results do not exceed 3% and the MAD do not exceed 3°C (only for HFE-7200, the maximum value of the MAD is equal to 3.93°C).

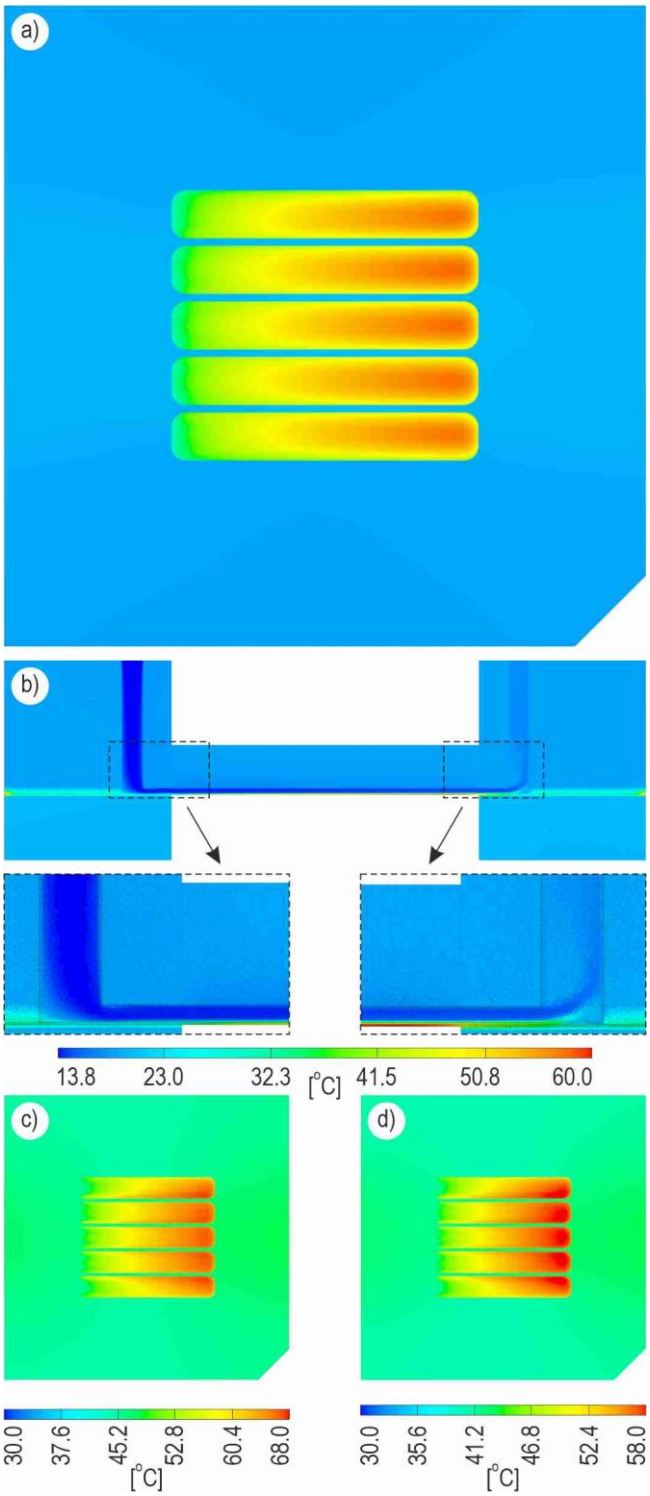

Fig. 4. Temperature distribution in the test section as the results of numerical computations in Simcenter STAR-CCM+, for experiments with fluids: HFE-649 (a,b), HFE-7100 (c) and HFE-7200 (d); (a) view on the side with the heated plate, (b) longitudinal section of the central minichannel; computational grids are visible in enlarged sections of the inlet (left side) and the outlet (right side)

Tab. 5. The MRD and MAD values determined on the basis of the Simcenter STAR-CCM+ results and the data from the experiments

Compared results	MRD (%)	MAD (°C)
HFE-649		
Temperature of an outer surface of the heated plate obtained by an infrared camera and by Simcenter STAR-CCM+	1.59	2.39
HFE-7100		
Temperature of on outer surface of the heated plate obtained by an infrared camera and by Simcenter STAR-CCM+	2.82	3.93
HFE-7200		
Temperature of the outer surface of the heated plate obtained by an infrared camera and by Simcenter STAR-CCM+	2.28	2.57

MAD, maximum absolute difference; MRD, mean relative differences.

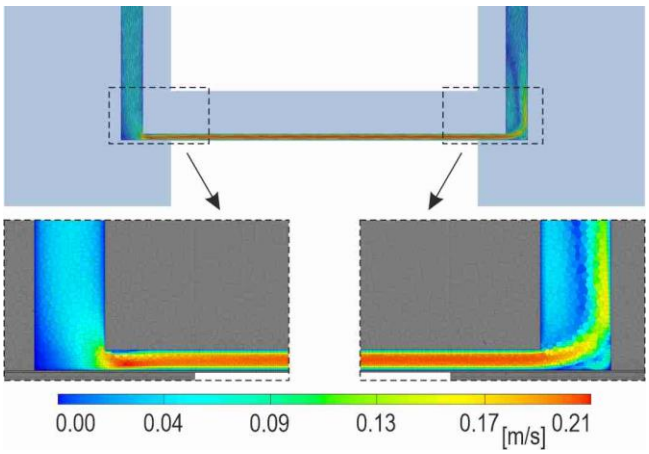

Fig. 5. Velocity distribution in the fluid obtained from numerical calculations by Simcenter STAR-CCM+ in the longitudinal section of the central minichannel based on the data from the experiment with HFE-649; computational grids are visible in enlarged sections of the inlet (left side) and the outlet (right side)

4.2. Simcenter STAR-CCM+ vs HPM and TM

The TM was used to determine the temperature of the heated plate at the contact surface with the working fluids. Moreover, the results from numerical simulation in the Simcenter STAR-CCM+, in the form of temperature plots at the heated plate-fluid interface, were also obtained and shown for comparison. The local heat transfer coefficients were also determined according to the proposed calculation methods. A 1D approach based on Fourier's law was utilised to validate the heat transfer coefficient results derived from the TM and the HPM with TM. According to Ref. [38], the local heat transfer coefficients were calculated from the following formula:

$$\alpha_{1D}(x) = \frac{q_V}{T_G(x,\delta_G) - T_{f,lin}(x) - q_V \delta_G \lambda_G^{-1}} \tag{11}$$

where $T_{f,lin}$ is the linearly changing fluid temperature from the inlet temperature to the outlet temperature.

The results of calculations based on the experimental data are presented against the distance from the minichannel inlet as follows:

– in Fig. 7, as the temperature of the contact heated plate – fluid surface according to the calculations using the TM and by Simcenter STAR-CCM+;
– in Fig. 8, as the heat transfer coefficient according to the calculations using the HPM with the TM and by Simcenter STAR-CCM+.

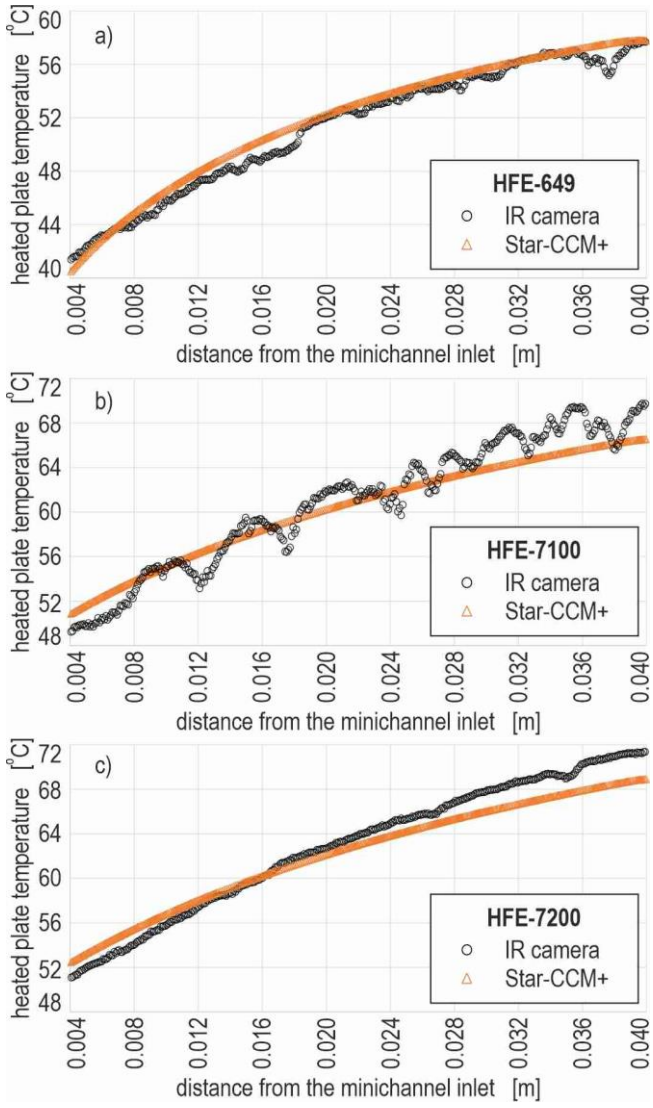

Fig. 6. Temperature of the heated plate on the outer surface contacting ambient air from the calculation performed in Simcenter STAR-CCM+ and obtained from the measurement due to an infrared camera, both as a function of the distance from the minichannel inlet

To compare the results from numerical simulations and calculations with the use of TM and the 1D approach, the differences in form of MAD and the maximum average relative differences (MARD) were determined.

MARD was defined by the following formula

$$\mathrm{MARD} = \max\left(\frac{\|f-g\|}{\|f\|}, \frac{\|f-g\|}{\|g\|}\right) \tag{12}$$

where: || || means L 2 norm.

Tables 6 and 7 show the fluids MARD and MAD values for the fluids under consideration and related to the contact surface temperatures and the calculated heat transfer coefficients.

The analysis of the temperature results shows that numerical simulations in Simcenter STAR-CCM+ yield similar results to those obtained from the experiment (Fig. 6) and methods based on Trefftz functions (Fig. 7) and the 1D approach. For both methods, i.e. the TM and simulations in Simcenter STAR-CCM+, similar temperature distribution patterns are observed, with minor differences in their values.

A comparative analysis of the results obtained from the two methods was carried out, the effects of which are shown in Fig. 7 and listed in Tab. 6. The MARD and MAD values determined between the temperature values at the plate–fluid interface, determined with the help of TM and the Simcenter STAR-CCM+ are listed in Tab. 6 The MARD values appear to be slight and are in the range 1.4%–2.28%. Furthermore, MAD values do not exceed 3 °C.

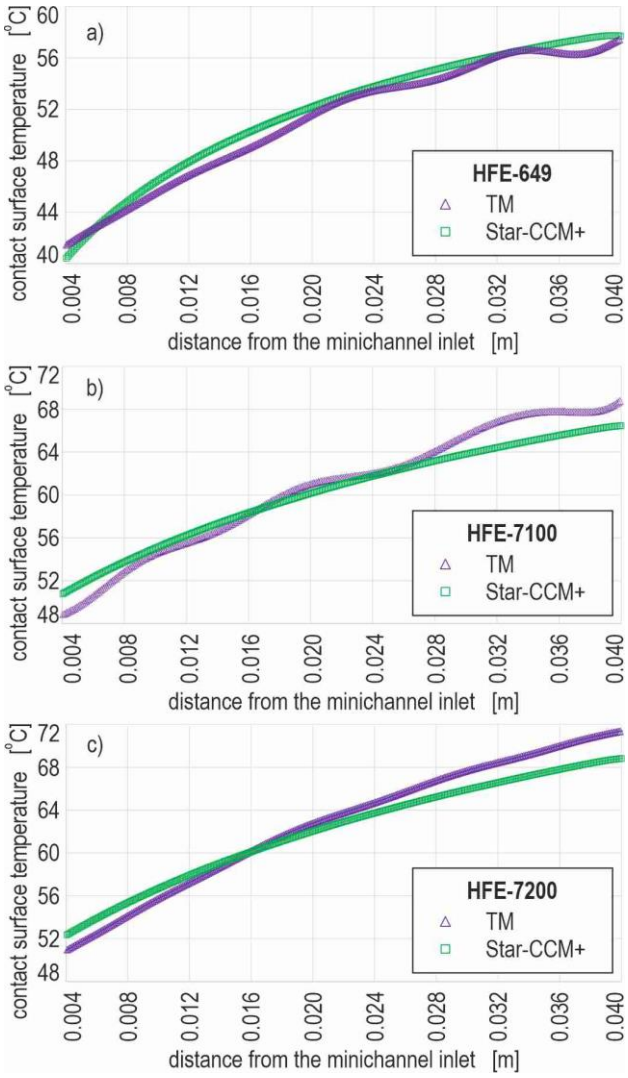

Fig. 7. Temperature of the contact heated plate-fluid surface according to the calculations using the TM and due to Simcenter STAR-CCM+ as a function of the distance from the minichannel inlet. TM, Trefftz method

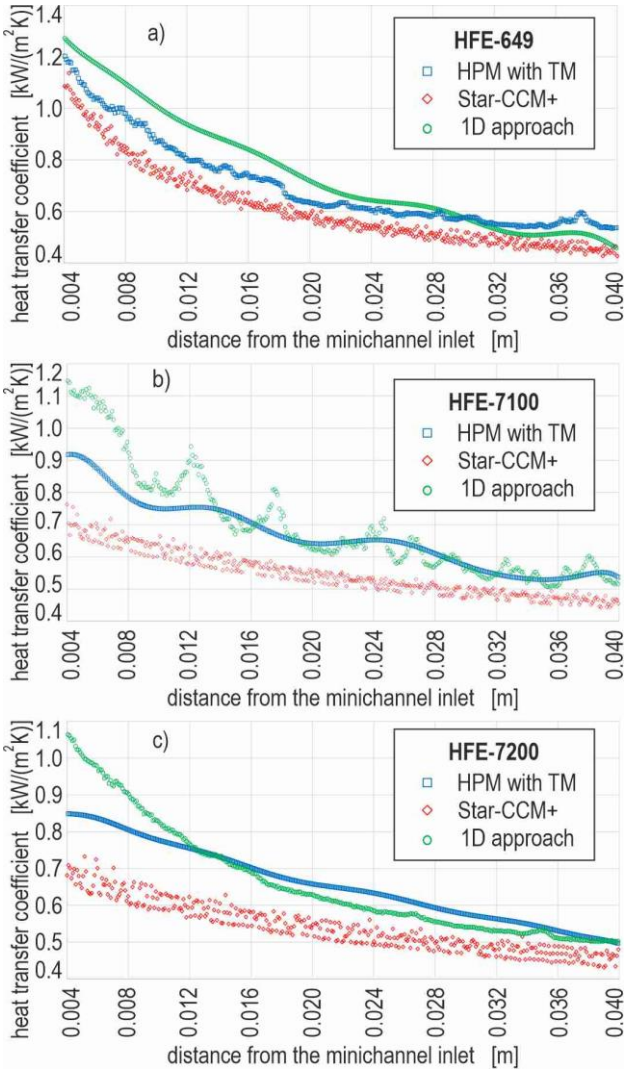

Fig. 8. Heat transfer coefficient according to the calculations using the HPM with the TM, Simcenter STAR-CCM+ and the 1D approach as a function of the distance from the minichannel inlet. HPM, homotopy perturbation method; TM, Trefftz method

Tab. 6. The MARD and the MAD values for calculated contact surface temperature

Compared results	MARD [%]	MAD [°C]
HFE-649		
Contact surface temperature from calculations by the TM and Simcenter STAR-CCM+	1.40	2.81
HFE-7100		
Contact surface temperature from calculations by the TM and Simcenter STAR-CCM+	2.28	2.81
HFE-7200		
Contact surface temperature from calculations by the TM and Simcenter STAR-CCM+	2.20	2.48

DOI 10.2478/ama-2024-0027

Tab. 7. The MARD and the MAD values between heat transfer coefficient values calculated from the proposed mathematical methods

Compared results	MARD [%]	MAD [W/(m^{2}K)]]
HFE-649		
Heat transfer coefficient obtained by the HPM with the TM and Simcenter STAR-CCM+	25.07	251.68
Heat transfer coefficient obtained by the HPM with the TM and 1D approach	21.64	131.08
Heat transfer coefficient obtained by the Simcenter STAR-CCM+ and 1D approach	14.26	128.29
HFE-7100		
Heat transfer coefficient obtained by the HPM with the TM and Simcenter STAR-CCM+	22.26	223.63
Heat transfer coefficient obtained by the HPM with the TM and 1D approach	11.03	227.95
Heat transfer coefficient obtained by the Simcenter STAR-CCM+ and 1D approach	32.34	451.58
HFE-7200		
Heat transfer coefficient obtained by the HPM with the TM and Simcenter STAR-CCM+	22.80	174.98
Heat transfer coefficient obtained by the HPM with the TM and 1D approach	9.43	227.17
Heat transfer coefficient obtained by the Simcenter STAR-CCM+ and 1D approach	27.31	387.81

The primary purpose of the HPM combined with the application of the TM was to determine the heat transfer coefficient. Analysis of the results in Fig. 8 shows that the coefficient takes the highest values at the minichannel inlet while the lowest values at the outlet. According to the dependences, it was noticed that the heat transfer coefficient decreases with distance from the minichannel inlet. Similar plots were achieved with respect to the results obtained from HPM with the TM compared to the results resulting from the Simcenter STAR-CCM+ simulations and the 1D approach. Furthermore, for the results obtained by the presented calculation methods, the MARDs are in the range 9.43%–32.34% and the MAD did not exceed 451.58 W/(m2K) (see Tab. 7).

Generally, it was stated that the high agreement between the experimental results and those obtained with the TM and 1D approach allows for the validation of the CFD model.

When the heat transfer coefficient values determined from the combination of the HPM with the TM, Simcenter STAR-CCM+ and 1D approach were analysed, it was noticed that similar heat results were achieved. The highest value of the calculated difference between the heat transfer coefficients (262.68 W/(m2K)) according to both computational approaches occurred near the channel inlet. It could also be underlined that the same relationship was obtained between the heat transfer coefficient and the distance from the minichannel inlet. With increasing distance from the inlet, the heat transfer coefficient decreased not dependently on the type of a cooling fluid.

5. CONCLUSIONS

The main aim was to develop an effective method to identify the heat transfer coefficient at the heater–working fluid interface during its flow in a minichannel. Numerical studies of heat transfer were based on experimental data concerning cooling fluid flow in a group of five 1-mm deep minichannels. The selected data from the experimental series relate the single-phase forced convection and the start of subcooled boiling. A two-dimensional mathematical model was developed, which assumed steady state heat transfer
in the test section. The 1D approach allowed for the validation of heat transfer coefficients determined according to the Trefftz functions and numerical calculation in CFD.

Two methods based on Trefftz functions, i.e. the classical TM and the HPM, were used to determine the temperature of the heated plate and the fluid. The advantage of the methods based on Trefftz functions used in the work is the simple mathematical apparatus. It was sufficient to use a small number of Trefftz functions and a few iterations to obtain satisfactory results. Methods based on Trefftz functions were compared with the results obtained with commercial CFD software, Simcenter STAR-CCM+ and the 1D approach.

The main findings from the analysis of the results are as follows.

- the temperature distribution on the heated plate obtained from numerical simulations was consistent with the temperature distribution achieved experimentally and determined by the TM. The MRD do not exceed 3% and the MAD was below 4°C. The high agreement between the experimental results and those obtained with the TM allows for the validation of the CFD model;
- the comparison between the heat transfer coefficients, calculated by the presented calculations methods gave satisfactory results;
- the use of combination of the HPM with the TM and Simcenter STAR-CCM+ yielded similar heat transfer coefficient values; the most significant differences reaching 251.68 W/(m2K) were observed near the minichannel inlet;
- from computational approaches, a similar plot of heat transfer coefficient variation as a function of distance from the minichannel inlet was obtained – the coefficient was found decreasing.

Comparison of the results obtained with the two presented calculation methods, i.e. simulation by CFD and methods with Trefftz functions, is the forte of this work. The 1D approach based on Fourier's law was utilised to validate the heat transfer coefficient results derived from the hybrid method HPM with TM and numerical simulations in Simcenter STAR-CCM+. It should be noted that the presented calculations are based on experimental data. Furthermore, comparison of the results by the Simcenter STAR-CCM+ program with experimental measurements made it possible to validate the model adopted in this program. As a result of the validation of the aforementioned model, further studies including other refrigerants could allow for reduction of the experimental part in favour of numerical simulations. Both steady-state and time-dependent problems will be considered, and the CFD software will also be used for their analysis.

Nomenclature:

cp – specific heat capacity, J/(kg K)
f, g – functions
H – length of the minichannel, m
h – function
HPM – homotopy perturbation method
L – linear operator

M – number of terms in Taylor series
MAD – maximum absolute difference
MARD – maximum average relative difference
MRD – mean relative differences
N – nonlinear operator
p – parameter
qV – volumetric heat flux, W/m3
T – temperature, K
TM – Trefftz method
u0 – initial approximation of the solution
w – velocity, m/s
x – coordinate in the direction of flow, m
y – coordinate in the direction perpendicular to the flow and width of the partitions, m

Greek letters:
α – heat transfer coefficient, W/(m2 K)
δ – thickness, depth, m
λ – thermal conductivity, W/(m K)
ρ – density, kg/m3

Subscripts:
ave – average
f – fluid
G – heated plate
in – inlet
IR – infrared camera
lin – linear
M – minichannel
out – outlet
1D – one dimension

REFERENCES

1. Tibirica CB, Ribatski G. Flow boiling in micro-scale channels - Synthesized literature review. International Journal of Refrigeration. 2013;36(2): 301-324. https://doi.org/10.1016/j.ijrefrig.2012.11.019
2. Da Silva PF, de Oliveira JD, Copetti JB, Macagnan MH, Cardoso EM. Flow boiling pressure drop and flow patterns of R-600a in a multiport minichannels. International Journal of Refrigeration. 2023;148: 13-24. http://doi.org/10.1016/j.ijrefrig.2023.01.001
3. Wang D, Wang D, Hong F, Xu J, Zhanga C. Experimental study on flow boiling characteristics of R-1233zd(E) of counter-flow interconnected minichannel heat sink. International Journal of Heat and Mass Transfer. 2023;215(124481):1-19. https://doi.org/10.1016/j.ijheatmasstransfer.2023.124481
4. Rafałko G, Grzybowski H, Dzienis P, Zaborowska I, Mosdorf R, Litak G. Recurrence analysis of phase distribution changes during boiling flow in parallel minichannels. The European Physical Journal Special Topics. 2023;232: 201-207. https://doi.org/10.1140/epjs/s11734-022-00741-0
5. Saghir MZ, Alhajaj Z. Optimum multi-mini-channels height for heat enhancement under forced convection condition. Energies. 2021;14(7020):1-13. https://doi.org/10.3390/en14217020
6. Piasecka M, Piasecki A, Dadas N. Experimental Study and CFD Modeling of Fluid Flow and Heat Transfer Characteristics in a Mini-channel Heat Sink Using Simcenter STAR-CCM+ Software. Energies. 2022;15(536):1-20. https://doi.org/10.3390/en15020536
7. Piasecka M, Strąk K. Influence of the Surface Enhancement on the Heat Transfer in a Minichannel. Heat Transfer Engineering. 2019;40(13-14): 1162-1175. https://doi.org/10.1080/01457632.2018.1457264
8. Piasecka M, Maciejewska B, Łabędzki P. Heat Transfer Coefficient Determination during FC-72 Flow in a Minichannel Heat Sink Using the Trefftz Functions and ADINA Software. Energies. 2020;13(6647): 1-25. https://doi.org/10.3390/en13246647
9. Hadamard J. Sur les Problèmes aux Dérivées Partielles et Leur Signification Physique. Princet. Univ. Bull. 1902;13: 49–52.
10. Kurpisz K, Nowak AJ. Inverse Thermal Problems. Southampton, UK and Boston: Computational Mechanics Publications; 1995.
11. Bakushinskii A, Goncharsky A. Ill-Posed Problems:Theory and Applications. Dordrecht: Kluwer; 1995.
12. Tikhonov AN, Goncharsky AV, Stepanov VV, Yagola AG. Numerical Methods for the Solution of Ill-Posed Problems. London: Kluwer Academic; 1990.
13. Lesnic D. Inverse Problems with Applications in Science and Engineering. New York: Chapman and Hall/CRC; 2021. https://doi.org/10.1201/9780429400629
14. Belgacem Ben F, El Fekih H. On Cauchy's Problem: I. A Variational Steklov-Poincar´e Theory. Inverse Problems. 2005;21:1915–1936. https://doi.org/10.1088/0266-5611/21/6/008
15. Ciałkowski MJ, Frąckowiak A, Grysa K. Solution of a stationary inverse heat conduction problems by means of Trefftz non-continuous method. International Journal of Heat and Mass Transfer. 2007;50: 2170-2181. https://doi.org/10.1016/j.ijheatmasstransfer.2006.11.030
16. Maciąg A, Grysa K. Temperature dependent thermal conductivity determination and source identification for nonlinear heat conduction by means of the Trefftz and Homotopy perturbation methods. International Journal of Heat and Mass Transfer. 2016;100: 627-633. https://doi.org/10.1016/j.ijheatmasstransfer.2016.04.103
17. Ciałkowski MJ, Grysa K. A sequential and global method of solving an inverse problem of heat conduction equation. Journal of Theoretical and Applied Mechanics. 2010;48(1): 111-134.
18. Liu CS. A modified collocation Trefftz method for the inverse Cauchy problem of Laplace equation. Engineering Analysis with Boundary Elements. 2008;32(9):778-785. https://doi.org/10.1016/j.enganabound.2007.12.002
19. Qin QH. The Trefftz Finite and Boundary Element Method. Southampton: WIT Press; 2000.
20. Grysa K, Maciąg A. Homotopy perturbation method and Trefftz functions in the source function identification. Singapore: APCOM&ISCM, 2013 Dec 11-14.
21. Hożejowska S. Homotopy perturbation method combined with Trefftz method in numerical identification of liquid temperature in flow boiling. Journal of Theoretical and Applied Mechanics. 2015;53(4): 969-980. https://doi.org/10.15632/jtam-pl.53.4.969
22. Maciąg A, Pawińska A. The solution of nonlinear direct and inverse problems for beam by means of the Trefftz functions. European Journal of Mechanics - A/Solids. 2022;92:1-6. https://doi.org/10.1016/j.euromechsol.2021.104476
23. Trefftz E. Ein Gegenstück zum Ritzschen Verfahren. 2 Int. Kongress für Technische Mechanik. 1926: 131-137.
24. Hożejowska S, Hożejowski L, Piasecka M. Radial basis functions in mathematical modelling of flow boiling in minichannels. EPJ Web of Conferences. 2017;143(02037):1-5.
25. Zhao X, Li JM, Riffat SB. Numerical study of a novel counter-flow heat and mass exchanger for dew point evaporative cooling. Applied Thermal Engineering. 2008;28:1942-1951. https://doi.org/10.1016/j.applthermaleng.2007.12.006
26. Zibart A, Kenig EY. Numerical investigation of conjugate heat transfer in a pillow-plate heat exchanger. International Journal of Heat and Mass Transfer. 2021;165(120567):1-17. https://doi.org/10.1016/j.ijheatmasstransfer.2020.120567
27. Gorobets V, Trokhaniak V, Bohdan Y, Antypov I. Numerical Modeling of Heat Transfer and Hydrodynamics in Compact Shifted Arrangement Small Diameter Tube Bundles. Journal of Applied and Computational Mechanics. 2021;7(1):292-301. https://doi.org/10.22055/jacm.2020.31007.1855
28. Lee W-J, Jeong JH. Development of a numerical analysis model for a multi-port minichannel heat exchanger considering a two-phase flow distribution in the header. Part I: Numerical modelling. International Journal of Heat and Mass Transfer. 2019;138: 1264-128 https://doi.org/10.1016/j.ijheatmasstransfer.2019.04.100

29. Adam A, Han D, He W, Chen J. Numerical analysis of cross-flow plate type indirect evaporative cooler: Modeling and parametric analysis. Applied Thermal Engineering. 2021;185(116379):1-13. https://doi.org/10.1016/j.applthermaleng.2020.116379
30. Ayli E, Bayer O, Aradag S. Experimental investigation and CFD analysis of rectangular profile FINS in a square channel for forced convection regimes. International Journal of Thermal Sciences. 2016;109: 279-290. https://doi.org/10.1016/j.ijthermalsci.2016.06.021
31. Mu Y-T, Chen L, He Y-L, Tao W-Q. Numerical study on temperature uniformity in a novel mini-channel heat sink with different flow field configurations. International Journal of Heat and Mass Transfer. 2015;85: 147-157 https://doi.org/10.1016/j.ijheatmasstransfer.2015.01.093
32. https://www.3m.com/3M/en_US/p/d/b5005005025/
33. https://www.3m.com/3M/en_US/p/d/b40044867/
34. https://www.3m.com/3M/en_US/p/d/b40045142/
35. https://www.3m.com/
36. Piasecka M, Hożejowska S, Maciejewska B, Pawińska A. Time-dependent heat transfer calculations with Trefftz and Picard methods for flow boiling in a mini-channel heat sink. Energies. 2021;14: 1-24. https://doi.org/10.3390/en14071832
37. Biazar J, Ghazvini H. Convergence of the homotopy perturbation method for partial differential equations. Nonlinear Analysis: Real World Applications. 2009;10: 2633-2640. https://doi.org/10.1016/j.nonrwa.2008.07.002
38. Piasecka M, Strąk K. Characteristics of Refrigerant Boiling Heat Transfer in Rectangular Mini-Channels during Various Flow Orientations. Energies. 2021;14(4891):1-29. https://doi.org/10.3390/en14164891

The research reported herein was funded by the National Science Centre, Poland, grant no. UMO-2018/31/B/ST8/01199.

Anna Pawińska: https://orcid.org/0000-0002-1949-9433

Artur Piasecki: https://orcid.org/0009-0002-7870-5951

Norbert Dadas: https://orcid.org/0000-0001-9241-6158

Sylwia Hożejowska: https://orcid.org/0000-0003-2558-5132

Magdalena Piasecka: https://orcid.org/0000-0003-3696-6213